Journal of Biomechanics 157 (2023) 111725

Contents lists available at ScienceDirect

Journal of Biomechanics

journal homepage: www.elsevier.com/locate/jbiomech

Cosimulation of the index finger extensor apparatus with finite element and musculoskeletal models

Christopher T. Jadelis [a,*], Benjamin J. Ellis [c], Derek G. Kamper [a,b], Katherine R. Saul [a]

[a] North Carolina State University, Raleigh, NC, United States
[b] University of North Carolina, Chapel Hill, NC, United States
[c] Department of Biomedical Engineering, and Scientific Computing and Imaging Institute, University of Utah, Salt Lake City, UT, United States

A B S T R A C T

Musculoskeletal modeling has been effective for simulating dexterity and exploring the consequences of disability. While previous approaches have examined motor function using multibody dynamics, existing musculoskeletal models of the hand and fingers have difficulty simulating soft tissue such as the extensor mechanism of the fingers, which remains underexplored. To investigate the extensor mechanism and its impact on finger motor function, we developed a finite element model of the index finger extensor mechanism and a cosimulation method that combines the finite element model with a multibody dynamic model. The finite element model and cosimulation were validated through comparison with experimentally derived tissue strains and fingertip endpoint forces respectively. Tissue strains predicted by the finite element model were consistent with the experimentally observed strains of the 9 postures tested in cadaver specimens. Fingertip endpoint forces predicted using the cosimulation were well aligned in both force (difference within 0.60 N) and direction (difference within 30° with experimental results. Sensitivity of the extensor mechanism to changes in modulus and adhesion configuration were evaluated for ± 50% of experimental moduli, presence of the radial and ulnar adhesions, and joint capsule. Simulated strains and endpoint forces were found to be minimally sensitive to alterations in moduli and adhesions. These results are promising and demonstrate the ability of the cosimulation to predict global behavior of the extensor mechanism, while enabling measurement of stresses and strains within the structure itself. This model could be used in the future to predict the outcomes for different surgical repairs of the extensor mechanism.

1. Introduction:

Manual dexterity is essential for activities of daily living and has thus been a focus of disability research (Duruöz, 2014). Musculoskeletal modeling of the hand has been one strategy to study disability affecting the upper limb by enabling identification of contributions of individual muscles and passive tissues to motion and force production (Barry et al., 2018; Binder-Markey et al., 2019; Binder-Markey and Murray, 2017; Kamper et al., 2002). Because of the relatively small inertia of the finger segments, passive forces arising from soft tissue structures are especially important to the stability of hand movements (Binder-Markey and Murray, 2017). Previous attempts have been made to model contributions of soft tissues, such as representing joint capsules and tendinous or ligamentous adhesions in the hand through passive joint stiffness, modeled as torsional spring-damper elements (Barry et al., 2018; Binder-Markey and Murray, 2017). These approaches however, have been limited, as most current musculoskeletal modeling techniques that make use of multibody dynamics, such as OpenSim (Delp et al., 2007), rely on lumped parameter musculotendon models. These platforms are not capable of modeling heterogeneous structures that interact with multiple tendons and bones.

One such structure is the extensor mechanism, an aponeurosis running the length of each finger along the dorsal side. Multiple tendons from extrinsic extensor and intrinsic muscles of the hand integrate with this structure, forming a compound tendinous sheath with variable material properties (Garcia-Elias et al., 1991; Qian et al., 2014). The extensor mechanism terminates at the central slip (CS) and terminal slip (TS) tendinous insertions, present at the proximal end of the middle and distal phalanges, respectively (Lee et al., 2008; Qian et al., 2014), while also interacting with the phalanges through anatomical adhesions that restrict extensor mechanism displacement. Because of its branching architecture and heterogeneous material properties, the extensor mechanism is best represented through finite element (FE) analysis (Elyasi et al., 2017), which allows estimation of forces present at the adhesion and insertion sites. The use of an FE model additionally enables simulation of tendon injury and finger deformity. Tendon injuries have been shown to alter adhesion behavior in the extensor mechanism due to scar formation following injury, resulting in an altered force distribution, extensor lag and loss of extensor function (Colzani et al., 2016; Gangatharam and Leblanc, 2013). Using a FE model enables the direct

* Corresponding author at: Christopher Jadelis, MS Graduate Research Assistant, North Carolina State University, 911, Oval Drive, Campus Box 7910, Raleigh, North Carolina 27695-7910, United States.
E-mail address: ctjadeli@ncsu.edu (C.T. Jadelis).

https://doi.org/10.1016/j.jbiomech.2023.111725
Accepted 11 July 2023
Available online 13 July 2023

modeling of altered adhesion behavior and changes in anatomy.

However, because FE analysis is more computationally expensive than other musculoskeletal modeling techniques, multibody dynamic simulations are more appropriate for capturing coordinated movement of the multibody system. Therefore, a cosimulation approach is desirable to leverage the benefits of both approaches. While cosimulation of this type has been applied in the lower limb (Schmitz and Piovesan, 2016) and shoulder (Dixit et al., 2020), it has not yet been applied to the type of structure and multi-joint anatomy present in the extensor mechanism and finger.

The objective of this work was to develop and evaluate a FE model of the index finger extensor mechanism and a cosimulation using the FE model with a multibody dynamic musculoskeletal model. This method incorporates the multi-insertion behavior of the extensor mechanism using FE analysis while maintaining the computational efficiency of the multibody dynamic musculoskeletal model for dynamic simulations. We hypothesized that simulations of the index finger extensor mechanism using a FE model within cosimulation would predict tissue strains and fingertip endpoint forces comparable to those measured in cadaveric studies (Lee et al., 2008; Qiu, 2014). We also expected that the cosimulation model using anatomic extensor mechanism tissue representations would yield endpoint forces comparable to those produced using multibody musculoskeletal models that directly specify equivalent musculoskeletal geometry (moment arms) (Barry et al., 2018).

2. Methods:

2.1. Finite element model development

To model the tissue mechanics of the extensor mechanism, a FE model of the index finger extensor mechanism was developed (Fig. 1b) using magnetic resonance (MR) images of a single cadaver hand. The MR images were manually segmented (Amira image processing software, Visage Imaging, Inc., San Diego, CA) into bone and soft tissue, and meshed using a FE preprocessor (TrueGrid, XYZ Scientific Applications, Inc., Livermore, CA). The extensor mechanism was modeled as a deformable mesh composed of four-node quadrilateral shell elements, while the phalanges were treated as rigid bodies using triangular shell elements. The discretization of the extensor mechanism was verified with a convergence study and the phalanges were discretized with a sufficient number of elements to create smooth contact surfaces. FEBio Studio (Maas et al., 2012) was used for the application of material properties and simulation studies.

To model the heterogeneous material properties of the extensor mechanism, the deformable mesh was partitioned into regions (Fig. 1b), each assigned an isotropic elastic material model represented as a Saint Venant-Kirchhoff model with region-specific material properties (Qian et al., 2014) (Table 1). These regions included the central band, lateral bands, sagittal tendon, CS, and TS. The deformable mesh is prevented from penetrating into the rigid body bones through the use of a sliding elastic contact constraint. Tendinous and ligamentous adhesions present on the ulnar and radial sides of the index finger were modeled using discrete tension-only spring elements to connect the extensor mechanism to the proximal phalanx and prevent separation. Similarly, the CS insertion and joint capsule adhesion present at the proximal interphalangeal joint (PIP) were modeled using tension-only springs between the extensor mechanism and medial phalanx. To facilitate modeling of specific finger postures, single degree-of-freedom (DOF) revolute joints were placed at the centers of rotation of the metacarpophalangeal (MCP), PIP, and distal interphalangeal (DIP) joints. The joint centers and axes of rotation of the single DOF joints were aligned to reproduce the non-orthogonal axes of rotation present in the index finger joints as defined in (Barry et al., 2018), and anthropometric proportions were evaluated for consistency. The axes in both the multibody and FE model

Table 1
Extensor Mechanism Material Properties (Qian et al., 2014).

Extensor mechanism Sample Location	Tangent Modulus (MPa)
Lateral Bands	105.38 ± 85.06
Soft Tendon (Sagittal Band)	54.68 ± 14.13
Central Slip	100.76 ± 46.77
Terminal Slip	89.67 ± 48.29
Extensor Tendon (Central Band)	100.61 ± 50.82

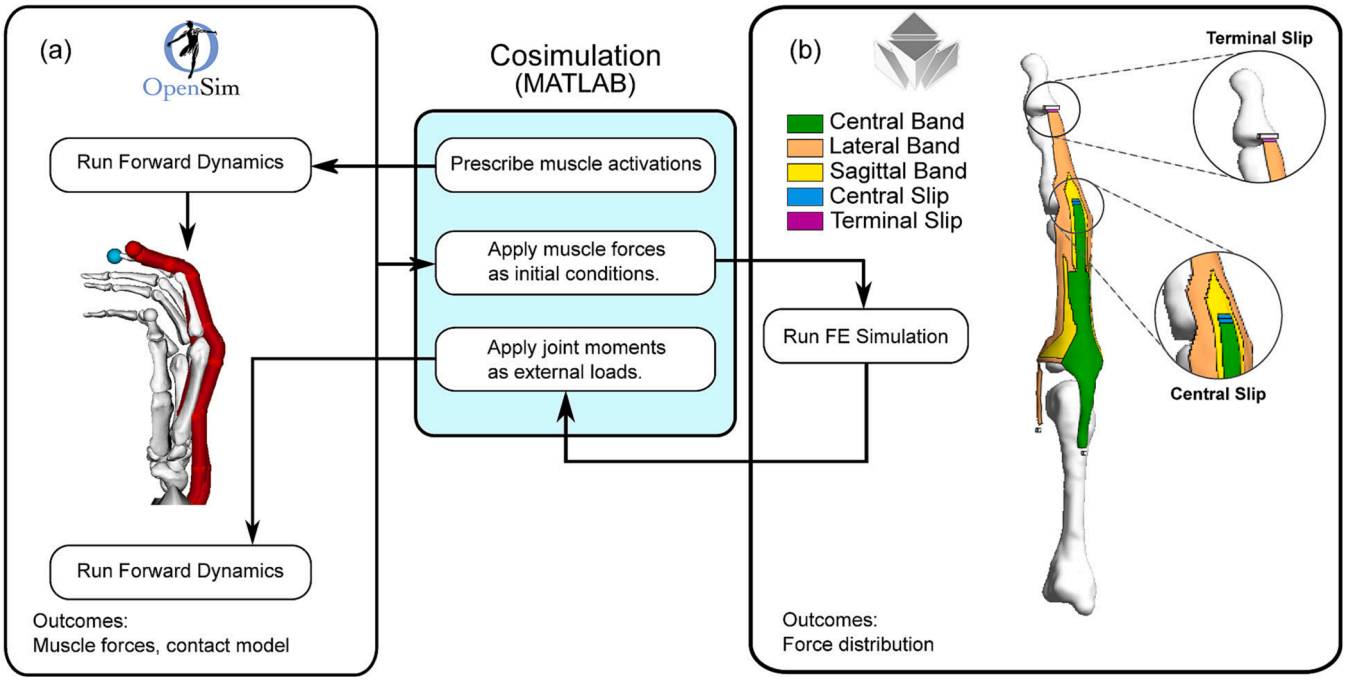

Fig. 1. Cosimulation framework including a) rigid body dynamic modeling and b) finite element modeling. A custom MATLAB program (center) passes information between the two simulation platforms.

were defined using the effective axes of rotation identified from cadaver specimens during flexion and extension (Hollister and Giurintano, 1993). The MCP also experiences abduction–adduction; however, for this study this axis was locked. To confirm the joint centers and rotation axes were aligned each model, we overlay the bones and axes from the OpenSim model with those from the FE model in two postures: resting (MCP = PIP = DIP = 0°) and experimental (MCP = 30°, PIP = 45°, DIP = 15°). Model registration was achieved by aligning the long axis of the metacarpal of the index finger (measured from the center of the base of the metacarpal to the center of the head of the metacarpal bone) for both model images and measuring the angular offset of each phalangeal bone from a top-down and side facing view using the sketch utility included in CAD software (Fusion 360, Autodesk Inc.). There were no discernable differences between the two models for joint rotation in either posture. To model tendon force on the extensor mechanism, the desired tendon forces were applied as rigid force constraints to rigid bodies fixed to the residual ends of the extensor digitorum communis tendon (EDC), the first palmar interosseous tendon (FPI) and the lumbrical tendon (LUM).

2.2. Finite element model validation

To evaluate the strain predictions from the model, simulations were conducted to replicate the loading and posture conditions in cadaver experiments (Lee et al., 2008). These were implemented in the FE model via prescribed joint rotations matching the experimental postures (Table 2) and a force of 11.8 N applied to the residual tendon of EDC, as performed in the experimental procedure. Relative longitudinal strains were recorded for the CS and TS insertions in each posture as prescribed in the experimental study (Equation 1). In this method, the strains for CS and TS are obtained by measuring the distance between proximal and distal nodes encompassing the CS and TS material regions, respectively (Fig. 2), in a given posture (i): when unloaded (l_o^i), during loading (l_f^i), and as compared to this distance in an unloaded neutral posture (l_o^1)(c.f. Posture 1, Table 2).

$$\widehat{\epsilon}_i = \frac{l_f^i - l_o^i}{l_o^1}$$

2.3. Multibody dynamic musculoskeletal model

A previously developed musculoskeletal model of the distal upper limb, hand, index finger, and thumb (Barry et al., 2018) was used as a foundation for the simulations described here and development of the cosimulation approach (Fig. 1a). This model was developed in OpenSim (v3.3) (Delp et al., 2007) and includes 17 muscles including 7 muscles crossing the index finger, 8 muscles crossing the thumb, and two crossing the wrist. For the purposes of this study, only four muscles specifically actuating the index finger were considered, while the muscles actuating the wrist and thumb and wrist and thumb motion were locked. The four muscles crossing the index finger representing the extrinsic and intrinsic extensors follow carefully prescribed paths representing the effective muscle contributions to the extensor mechanism aponeurosis. This model was previously validated using experimental data from cadaveric studies for static force production at the fingertip in a constrained posture (Qiu, 2014).

To replicate the experimental conditions for fingertip force production, the index finger was constrained to a posture of 30° flexion for the MCP, 45° flexion for the PIP, and 15° flexion for the DIP. Fingertip forces in the original cadaveric study were recorded using a 6 DOF load cell; to replicate this in simulation, a spherical contact surface attached to the tip of the index finger was placed inside a hollow spherical contact mesh to facilitate measurement of fingertip forces. Four muscles actuating the index finger were considered: The EDC, extensor indicis (EI), FPI, and LUM. As in Barry et al., the muscles were represented using a Hill-type muscle model (Millard et al., 2013) with force-generating parameters derived from literature (Jacobson et al., 1992; Pearlman et al., 2004; Triandafilou et al., 2011; Zajac, 1989) (Table 3).

Table 2
Joint angles for nine experimental postures (Lee et al., 2008).

Posture / Joint	1	2	3	4	5	6	7	8	9
MCP	0°	0°	0°	30°	30°	30°	60°	60°	60°
PIP	0°	30°	45°	30°	45°	45°	30°	45°	45°
DIP	0°	20°	30°	20°	30°	30°	20°	30°	30°

2.4. Cosimulation approach

The cosimulation workflow for integrating the multibody dynamic and FE models was developed in MATLAB (MathWorks, 2019) to exchange muscle force and joint moment information between the OpenSim and FE models (Fig. 1). To develop muscle forces in the chosen posture, a forward dynamics simulation is first initiated in the OpenSim model using predefined muscle excitations. These excitations, defined as a time series of muscle activation percentages, are used to inform the first order activation dynamics and contraction dynamics model (Delp et al., 2007; Millard et al., 2013) present in the MBD model to develop muscle forces. These corresponding muscle forces are implemented as initial conditions to the FE model. Muscle forces developed for the EI muscle are applied to the same actuator as for the EDC muscle, as these muscles insert into the extensor mechanism along similar paths (Suwannakhan et al., 2016). A FE study then computes flexion/extension joint moments developed by the extensor mechanism acting on the rigid bodies within the FE model during finger flexion with the FE model starting from rest (MCP, PIP, DIP = 0°). These are mapped to the equivalent coordinate system and units present in the OpenSim model, and applied to the OpenSim model as external torques at the MCP, PIP, and DIP joints in place of muscle actuators to capture the net effect of the complex extensor mechanism in the context of the multibody dynamic model.

2.5. Cosimulation and validation

To validate the cosimulation method, we performed a set of simulations to replicate fingertip force generation experiments conducted previously in cadavers (Qiu, 2014). In these experiments, loads were applied to cadaver tendons and the resulting three-dimensional force was measured at the fingertip. Forward dynamics simulations for our study were performed using the multibody dynamic model in a single constrained posture (MCP = 0°, PIP = 45°, and DIP = 30°). Each of the four musculotendon units considered (EDC, EI, FPI, and LUM) was independently actuated to generate 10% of the corresponding maximum isometric force. These musculotendon forces were independently applied as initial conditions to the FE model as described above. As only fingertip forces produced by muscle actuation were measured in the cadaver study (Qiu, 2014), an additional simulation was performed to record loads in the FE model produced from the passive forces resulting purely from posture changes. These results were subtracted from the previous simulations involving both muscle actuation and passive forces to isolate the effects of muscle actuation.Sensitivity analysis.

The FE model was developed from a single cadaver; material moduli and adhesion configuration within the extensor mechanism have been shown to vary among individuals (Qian et al., 2014; Ellis et al., 2011). Thus, multiple variations of the material moduli (Table 1) and adhesion properties (Fig. 1b) were simulated to evaluate their impact on slip strains and fingertip endpoint forces. The material modulus for each region was varied individually by ± 50% of the nominal modulus in 10% increments. This range was chosen to remain within the range of reported results, while also sufficiently perturbing materials that had relatively small standard deviations for the reported moduli. Adhesions were similarly varied for combinations with and without the radial and

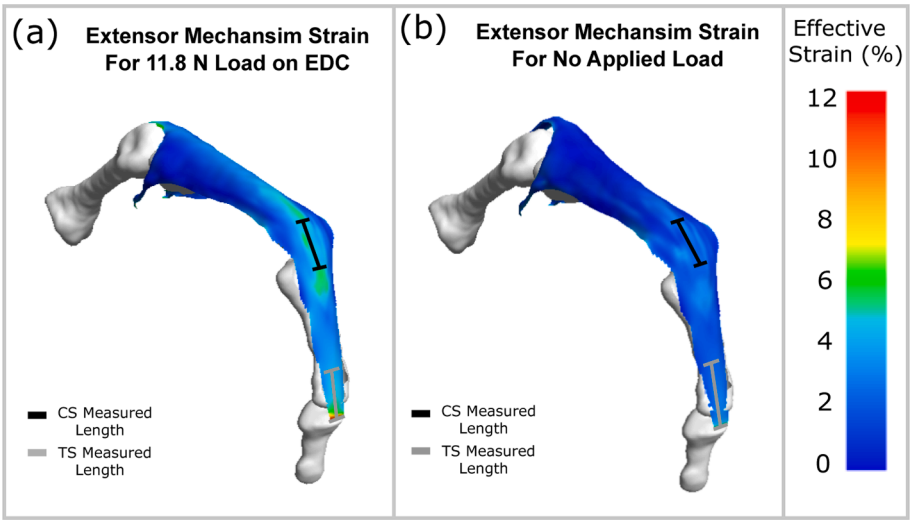

Fig. 2. Effective strain of the extensor mechanism (c.f. Posture 5, Table 2), with (a) 11.8 N load on the EDC tendon and (b) no load applied. Bars indicate measured strain region for CS (black) and TS (gray) (as in Equation 1).

Table 3
Multibody Dynamic Model Muscle Properties (Jacobson et al., 1992; Pearlman et al., 2004; Triandafilou et al., 2011; Zajac, 1989).

Muscle	f_o^m (N)	l_M^o (m)	l_S^T(m)	$\alpha(^\circ)$
Flexor Digitorum Profundis (FDP)	79.12	0.075	0.26812	7
Flexor Digitorum Superficialis (FDS)	58.9	0.084	0.29932	6
First Dorsal Interosseous medialis (FDIm)	72.8	0.030	0.02520	15
First Dorsal Interosseous lateralis (FDIl)	72.8	0.033	0.02569	15
Extensor Digitorum Communis (EDC)	34.69	0.070	0.26468	3
First Palmar Interosseous (FPI)	30.94	0.031	0.08978	6.3
Extensor Indicis (EI)	35.47	0.059	0.18479	6
Lumbrical (LUM)	25.04	0.068	0.05470	1.2

ulnar adhesions of the proximal phalanx, and with and without the joint capsule present at the central slip. The adhesion variations were performed with nominal material moduli. This analysis was only performed for the cosimulation to evaluate the effect of adhesions on endpoint forces. Slip strains calculated for the nominal and varied modulus cases were compared to experimental slip strains in each of the 9 postures described in the FE validation. The range of simulated slip strains in each posture for all moduli variations were reported in comparison to experimental slip strains. Fingertip endpoint forces were simulated for all material modulus and adhesion conditions. The net contact force vectors and magnitudes were compared to experimental endpoint forces (Qiu, 2014), and simulations created using only the OpenSim model. Contact force vectors and magnitudes were evaluated to examine the impact of material modulus and adhesion selection on endpoint forces and whether fingertip contact forces fell within the range of experimentally reported results.

3. Results

3.1. Finite element validation

Agreement between FE predicted strains and those measured in the experimental study (Lee et al., 2008) was high; for 8 of the 9 postures evaluated, the range of CS and TS strains predicted by the variation of moduli in the FE model were within one standard deviation of the experimentally measured strains (Fig. 3), with one posture (cf. Fig. 3, posture 8) falling outside of this range by 0.12% strain. The sensitivity analysis revealed that for variation in material modulus, the lateral bands were responsible for the largest variation in slip strain. Variation in modulus altered predicted slip strains, resulting in a range of 1.3% to

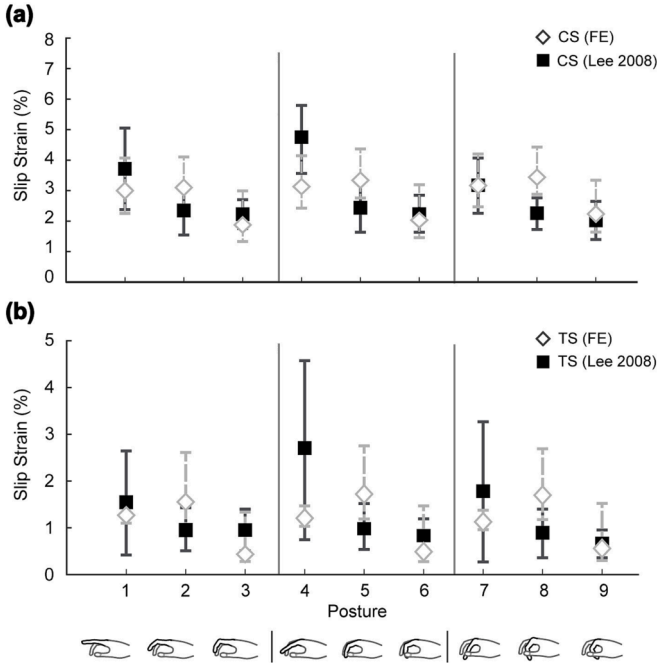

Fig. 3. Simulated and experimental CS and TS strains across all postures. Error bars present on experimental strains (dark grey) represent ± 1 standard deviation. Error bars on simulated strains (light grey) indicate maximum and minimum simulated range.

4.4% strain for the central slip, and 0.3% to 2.75% for the terminal slip (Fig. 3).

3.2. Cosimulation validation

Reported fingertip force magnitudes using the cosimulation method were consistent with experimentally reported results (Qiu, 2014), and were within 0.3 N in magnitude for the EDC, EI, and LUM muscles, and 0.60 N in magnitude for the FPI muscle for nominal material moduli (Fig. 4, Table 4). Variation in material modulus did not substantially affect force magnitudes; the largest observed difference was 0.07 N for the FPI muscle. Simulated fingertip force vectors in the sagittal plane for the EDC and EI muscles were directed proximally and dorsally in the

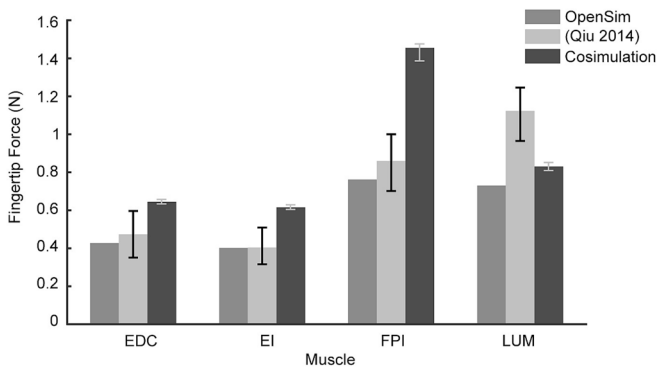

Fig. 4. Simulated fingertip contact force magnitudes for both the multibody dynamic model and cosimulation approach, in comparison to experimentally reported values (Qiu, 2014). Error bars for the experimentally reported values (black) indicate ± 1 standard deviation. Error bars on cosimulation values (light grey) indicate maximum and minimum simulated range.

reference frame of the distal phalanx (Fig. 5), thus consistent with simulations using the multibody dynamic model and experimentally reported results. The largest differences in direction between the cosimulation and experimental results were 18.3° and 30° for the EDC and EI muscles respectively, in the nominal modulus case (Fig. 5). The FPI and LUM muscles were directed distally and dorsally, consistent with the multibody dynamic simulation and experimental results, with a difference in direction for the cosimulation and experimental results of 12.4° and 0.6° for the FPI and LUM muscles respectively (Fig. 5). Variation in modulus did not affect the reported force directions for the cosimulation, with maximum reported deviations from the nominal properties of 3° for the EDC and EI muscles, and 2.1° and 0.7° for the FPI and LUM respectively.

Variation in adhesion configuration (Fig. 6) did not substantially affect fingertip force magnitudes, with a maximum change from the case with all adhesions of −0.14 N in the case where the radial and ulnar adhesions were removed. Adhesion configuration did substantially change fingertip force direction however, with removal of the joint capsule around the central slip contributing to a change in direction in the sagittal plane of −14.7° from the "all adhesions present" case. Similarly, removal of the joint capsule and radial and ulnar adhesions resulted in a change of −10.8° from the "all adhesions present" case.

4. Discussion:

The FE model converged across all 9 finger postures tested, demonstrating a wide range of finger flexion and extension joint angles able to be simulated. Predicted strain values coincided well with the range of strains recorded in a cadaver study examining the extensor mechanism (Lee et al., 2008), in accordance with our hypothesis. Variation in material moduli had appreciable effect on the reported strains in the central and terminal slips, with the range of simulated strains found to intersect with experimental strain ranges reported for multiple cadavers. The model predicted the observed pattern of decreasing strain with increasing flexion of the PIP and DIP joints. Large deviations from experimentally reported behavior were observed between model and cadaver strains however, at the terminal slip. As simulated TS strains fell within the experimentally reported range, this difference is likely due to a difference in material parameters between the cadaver specimen used to create the FE model, and the specimens used in the cadaver experiment. The material modulus has been shown to vary considerably

Table 4
Fingertip Force Magnitudes and Relative Differences.

Muscle	Experimental (Qiu 2014) (N)	OpenSim (N)	OpenSim (% Error)	Cosimulation (N)	Cosimulation (% Error)
EDC	0.47	0.43 (8.8%)	8.8	0.64 (36.2%)	36.2
EI	0.40	0.40 (0.6%)	0.6	0.63 (57.3%)	57.3
FPI	0.86	0.76 (11.6%)	11.6	1.48 (72.2%)	72.2
LUM	1.12	0.72 (35.8%)	35.8	0.84 (24.6%)	24.6

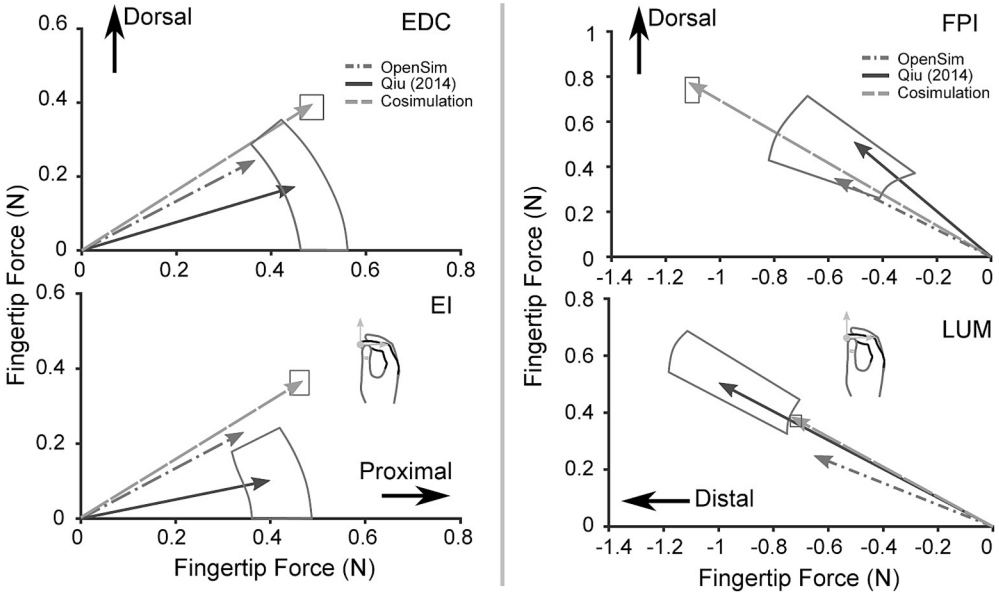

Fig. 5. Simulated fingertip force vectors for the EDC, EI, FPI, and LUM muscles in the sagittal plane for the multibody dynamic model, experimentally reported results (Qiu, 2014), and the cosimulation model. Error boundaries for experimental results indicate ± 1 standard deviation. Error boxes present for the cosimulation represent maximum and minimum simulated range.

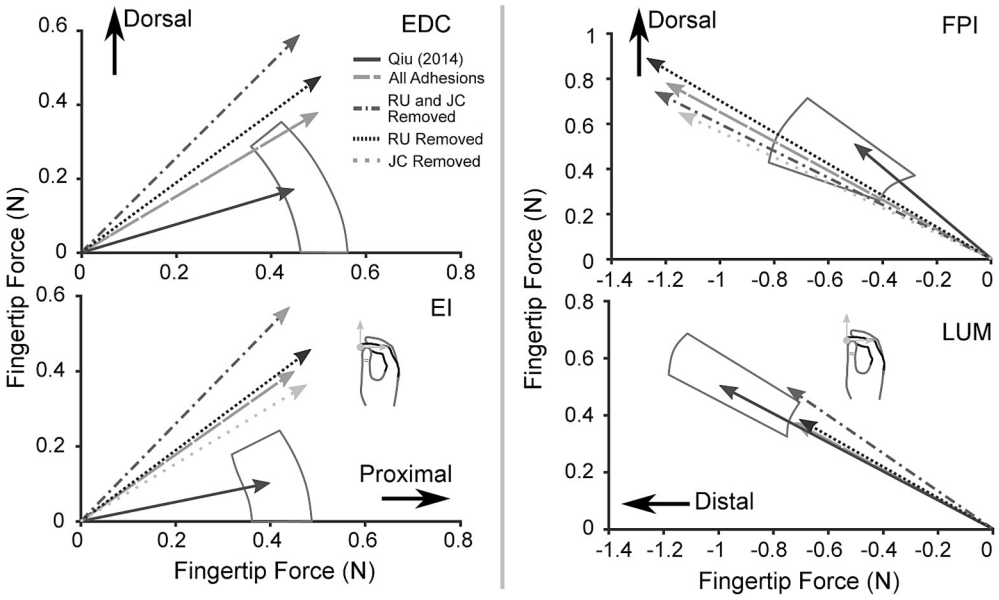

Fig. 6. Simulated fingertip force vectors for the EDC, EI, FPI, and LUM muscles in the sagittal plane in different adhesion configurations in comparison to experimentally reported results (Qiu, 2014). The abbreviations RU refer to the radial and ulnar adhesions present on the proximal phalange, and JC refers to the joint capsule present about the central slip.

between individuals (Qian et al., 2014).

It is also likely that discrepancies between simulated strains and experimental strains arose from the current material model and simplified joint representations implemented. Tendons are anisotropic (Yeh et al., 2012), with defined fiber directions, but the current FE model manages regional stiffness patterns through segmented regions only. As modulus oriented along the fiber was assumed to hold for all directions, internal forces and moments produced due to finger posture may be higher in the FE model than are observed physiologically. Additionally, single DOF joints used to represent rotation in the FE model may not fully capture physiologic joint behavior. Direct representation of fiber direction and anisotropy, and a more complex joint representation in future iterations of the FE model may allow for more accurate modeling and enable capture of additional features of force distribution and stiffness of the extensor mechanism. In addition, a hyperelastic model may improve performance. For example, our simulations predict relatively low net strains at the CS and TS in the nominal material modulus case, thereby suggesting that the nominal material properties are stiffer than the "effective" modulus according to the experimental stress strain curve and that in this strain regime the fibers may not be fully uncrimped (Qian et al., 2014). A different hyperelastic material model proposed by (Elyasi et al., 2017) may provide for a lower stiffness in this strain regime, while also accurately capturing deformations with higher strain.

The cosimulation model, combining the FE model of the extensor mechanism and the multibody dynamic model of the finger, was able to capture the soft tissue mechanics of the index finger extensor mechanism to inform dynamic simulations. The fingertip force vectors produced using cosimulation were similar to those produced by the multibody dynamic model, and recorded experimentally for all four muscles considered, with a maximum deviation of 30° in the sagittal plane from experimental results. Variation in material moduli did not produce a notable change in force vector direction, with a maximum reported deviation of 3°. This suggests that the extensor mechanism is not sensitive to changes in material modulus for production of fingertip forces. The cosimulation predicted force magnitudes within 0.3 N of experimental results (Qiu, 2014) for the EDC, EI, and LUM muscles, and 0.60 N for the FPI muscle, closely matching experimental results in absolute magnitude. However, the relative differences between experimentally measured and simulated force magnitudes are large, with the greatest difference in between experimental and simulated results being for the FPI, with a relative increase in magnitude of 72% for simulated results in comparison to experimentally measured values. These large relative differences may exist due to the small absolute magnitudes of experimental forces, and future validation of these models with larger experimental forces may improve accuracy. This is notable, as the magnitude of fingertip forces present in the experimental study (Qiu, 2014) were a maximum of 1.12 N for the LUM muscle (Table 4); however, previous studies (Goislard de Monsabert et al. 2012) have demonstrated that maximal fingertip forces for grip strength tasks may exceed 100 N, and tendon forces for individual muscles may additionally exceed 100 N. Thus, further validation under higher forces may yield would be beneficial and may yield more accurate results.

Variations in material modulus minimally impacted fingertip forces, with a maximum deviation of 0.07 N. Average fingertip force vectors fell outside of the ± one standard deviation used as acceptance criteria in the cadaver study (Qiu, 2014), but were generally well aligned with experimental data in terms of direction and magnitude. Simulation force direction for FPI activation was well aligned with the experimental data, but the magnitude was considerably larger for the cosimulation. The effective moment arm of the FPI muscle in the FE model may be larger than expected for each joint due to the behavior of the residual tendon, such that the ratio of the joint torques were correct, but the absolute values of the torques was too high. Additionally, dorsal-volar shifts in the extensor mechanism observed during flexion may not be captured in the model, and thus the effective static moment arm present in the model may not reflect the dynamic moment arm (Haines, 1951). In general, as the cadavers and sample sizes used for the studies of the collection of extensor material properties (Qian et al., 2014), fingertip force collection (Qiu, 2014), and creation of the MBD model (Barry et al., 2018), differed from the cadaver used in the generation of the FE model in this study, deviation from the experimental benchmark is expected.

Similarity between the cosimulation, multibody dynamic, and experimental results are encouraging, as muscle paths in the multibody dynamic model were carefully prescribed to replicate experimentally observed moment arms, while the FE model was developed using imaged anatomy and experimentally derived material properties. The

similarity in results between the cosimulation and multibody dynamic model suggests that the multi-insertion behavior of the FE model is able to replicate general behavior; the cosimulation model has the added benefit of allowing for additional insight into the deformation of the extensor mechanism, including measurement of forces at insertions and adhesions, which are unavailable using other techniques. Prior approaches for simulating the extrinsic extensors and intrinsic muscles that insert into the extensor mechanism require carefully prescribed moment arms, or are terminated at their effective insertion locations, which while useful, results in lost information due to interaction with the complex extensor mechanism (Barry et al., 2018; McFarland et al., 2021).

However, this additional insight into the behavior of the extensor mechanism made possible using a co-simulation approach does possess simulation and computational limitations that must be considered for use of this co-simulation in future studies. Implementation of the co-simulation over a MBD model or other simpler methods increases computation time and requires parameters that must be known beforehand, such as material parameters and anatomic data required to develop a finite element model. In the current configuration, a single simulation using the MBD model requires 6 min to complete, while a full co-simulation requires 15 min to complete using a desktop computer (Intel i5 4690 k, 16 GB RAM). Additionally, the MBD model in this co-simulation is used to develop muscle forces for use as initial conditions in the FE model. As the MBD model in this co-simulation does not consider the extensor hood, and instead models the effective contributions of each muscle through predefined paths, muscle forces developed by the MBD model may not fully reflect physiologic forces transmitted to the extensor mechanism. Thus it is important to consider the applicability of a cosimulation in future study design, as applications such as control of an exoskeleton where computational efficiency is essential may not benefit from the additional complexity introduced in a co-simulation. However, biomechanical studies and surgical planning, where computational efficiency is less important, may substantially benefit from the more granular information afforded by the inclusion of a cosimulation approach.

Other recent cosimulation approaches have incorporated FE models with multibody dynamic models to effectively examine knee ligament strain and tibiofemoral joint behavior during gait (Schmitz and Piovesan, 2016) and the progression of bone growth deformity in the upper limb following neural injury (Dixit et al., 2020). This study represents the first cosimulation to address the hand and incorporate the complex multi-joint and branching architecture of the finger and extensor mechanism. The approach is especially conducive to examination of hand neuromechanics due to the multi-articular nature of the finger tendons and their prevalent interactions with structures such as the anatomical pulleys and extensor mechanism (Kamper et al., 2006). Previous efforts have sought to model these structures through specified tendon routing (McFarland et al., 2021), a tendinous web approximation called “Winslow’s Rhombus” (Valero-Cuevas et al., 1998) (Leijnse and Spoor, 2012) (Valero-Cuevas et al., 2007), or elastic strings (Dogadov et al., 2017). In this work, we have presented a method for examining the extensor mechanism of the fingers in a more detailed fashion, allowing for the modeling of the branching architecture of this tissue, while integrating it with a larger multibody dynamic model. This approach potentially enables the study of larger coordinated dynamic motion of the forearm and hand while preserving detailed information about force distribution within the extensor mechanism.

CRediT authorship contribution statement

Christopher T. Jadelis: Conceptualization, Data curation, Writing - original draft, Writing - review & editing, Visualization, Investigation, Validation, Software. **Benjamin J. Ellis:** Conceptualization, Supervision, Resources, Software, Writing - review & editing. **Derek G. Kamper:** Conceptualization, Funding acquisition, Resources, Supervision, Writing - review & editing. **Katherine R. Saul:** Data curation, Conceptualization, Funding acquisition, Methodology, Project administration, Resources, Supervision, Writing – review & editing.

Declaration of Competing Interest

The authors declare that they have no known competing financial interests or personal relationships that could have appeared to influence the work reported in this paper.

Acknowledgements:

NSF IIS-2106747.

NIH 1R01NS052369-01A1.

We would also like to acknowledge Jimmy McDermott MS, for his support in troubleshooting the musculoskeletal model.

References:

Barry, A.J., Murray, W.M., Kamper, D.G., 2018. Development of a dynamic index finger and thumb model to study impairment. J. Biomech. 77, 206–210. https://doi.org/10.1016/j.jbiomech.2018.06.017.

Binder-Markey, B.I., Dewald, J.P.A., Murray, W.M., 2019. The biomechanical basis of the claw finger deformity: A computational simulation study. J. Hand Surg. Am. 44, 751–761. https://doi.org/10.1016/j.jhsa.2019.05.007.

Binder-Markey, B.I., Murray, W.M., 2017. Incorporating the length-dependent passive-force generating muscle properties of the extrinsic finger muscles into a wrist and finger biomechanical musculoskeletal model. J. Biomech. 61, 250–257. https://doi.org/10.1016/j.jbiomech.2017.06.026.

Colzani, G., Tos, P., Battiston, B., Merolla, G., Porcellini, G., Artiaco, S., 2016. Traumatic Extensor Tendon Injuries to the Hand: Clinical Anatomy, Biomechanics, and Surgical Procedure Review. J. Hand Microsurg. 8, 2. https://doi.org/10.1055/S-0036-1572534.

Delp, S.L., Anderson, F.C., Arnold, A.S., Loan, P., Habib, A., John, C.T., Guendelman, E., Thelen, D.G., 2007. OpenSim: Open-source software to create and analyze dynamic simulations of movement. IEEE Trans. Biomed. Eng. 54, 1940–1950. https://doi.org/10.1109/TBME.2007.901024.

Dixit, N.N., McFarland, D.C., Fisher, M.B., Cole, J.H., Saul, K.R., 2020. Integrated iterative musculoskeletal modeling predicts bone morphology following brachial plexus birth injury (BPBI). J. Biomech. 103 https://doi.org/10.1016/j.jbiomech.2020.109658.

Dogadov, A., Alamir, M., Serviere, C., Quaine, F., 2017. The biomechanical model of the long finger extensor mechanism and its parametric identification. J. Biomech. 58, 232–236. https://doi.org/10.1016/J.JBIOMECH.2017.04.030.

Duruöz, M.T., 2014. Assessment of Hand Functions. In: Hand Function. Springer New York, New York, NY, pp. 41–51. https://doi.org/10.1007/978-1-4614-9449-2_3.

Ellis, B., Wook Lee, S., Traylor, K., Weiss, J., Kamper, D., 2011. Impact of anatomical adhesions on stress distribution within the extensor hood of the index finger. American Society of Biomechanics Conference 2011.

Elyasi, N., Taheri, K.K., Narooei, K., Taheri, A.K., 2017. A study of hyperelastic models for predicting the mechanical behavior of extensor apparatus. Biomech. Model. Mechanobiol. 16, 1077–1093. https://doi.org/10.1007/S10237-017-0874-X.

Gangatharam, S., Leblanc, M., 2013. Alternate technique in managing adhesions after zone 3 extensor tendon repair: A case report. Tech. Hand Up. Extrem. Surg. 17, 46–48. https://doi.org/10.1097/BTH.0B013E31827878A1.

Garcia-Elias, M., An, K.N., Berglund, L.J., Linscheid, R.L., Cooney, W.P., Chao, E.Y.S., 1991. Extensor mechanism of the fingers. II. Tensile properties of components. J. Hand Surg. Am. 16, 1136–1140. https://doi.org/10.1016/S0363-5023(10)80080-2.

Goislard de Monsabert, B., Rossi, J., Berton, E., Vigouroux, L., 2012. Quantification of hand and forearm muscle forces during a maximal power grip task. Med. Sci. Sports Exerc. 44 (10), 1906–1916.

Haines, R.W., 1951. The extensor apparatus of the finger. J. Anat. 85, 251–259.

Hollister, A., Giurintano, D., 1993. How Joints Move, Clinical Mechanics of the Hand. Brand P Hollister Edt Mosby-Year b., 2nd. Ed. Inc St Louis Baltim.

Jacobson, M.D., Raab, R., Fazeli, B.M., Abrams, R.A., Botte, M.J., Lieber, R.L., 1992. Architectural design of the human intrinsic hand muscles. J. Hand Surg. Am. 17, 804–809. https://doi.org/10.1016/0363-5023(92)90446-V.

Kamper, D.G., George Hornby, T., Rymer, W.Z., 2002. Extrinsic flexor muscles generate concurrent flexion of all three finger joints. J. Biomech. 35, 1581–1589. https://doi.org/10.1016/S0021-9290(02)00229-4.

Kamper, D.G., Fischer, H.C., Cruz, E.G., 2006. Impact of finger posture on mapping from muscle activation to joint torque. Clin. Biomech. 21, 361–369. https://doi.org/10.1016/j.clinbiomech.2005.11.005.

Lee, S.W., Chen, H., Towles, J.D., Kamper, D.G., 2008. Effect of finger posture on the tendon force distribution within the finger extensor mechanism. J. Biomech. Eng. 130 https://doi.org/10.1115/1.2978983.

Leijnse, J.N.A.L., Spoor, C.W., 2012. Reverse engineering finger extensor apparatus morphology from measured coupled interphalangeal joint angle trajectories — a

generic 2D kinematic model. J. Biomech. 45, 569–578. https://doi.org/10.1016/J.JBIOMECH.2011.11.002.
Maas, S.A., Ellis, B.J., Ateshian, G.A., Weiss, J.A., 2012. FEBio: Finite elements for biomechanics. J. Biomech. Eng. 134 https://doi.org/10.1115/1.4005694.
MathWorks, 2019. MATLAB r2019b.
McFarland, D.C., Binder-Markey, B.I., Nichols, J.A., Wohlman, S.J., de Bruin, M., Murray, W.M., 2021. A Musculoskeletal Model of the Hand and Wrist Capable of Simulating Functional Tasks. bioRxiv 12 (28), 474357. https://doi.org/10.1101/2021.12.28.474357.
Millard, M., Uchida, T., Seth, A., Delp, S.L., 2013. Flexing computational muscle: Modeling and simulation of musculotendon dynamics. J. Biomech. Eng. 135 https://doi.org/10.1115/1.4023390.
Pearlman, J.L., Roach, S.S., Valero-Cuevas, F.J., 2004. The fundamental thumb-tip force vectors produced by the muscles of the thumb. J. Orthop. Res. 22, 306–312. https://doi.org/10.1016/j.orthres.2003.08.001.
Qian, K., Traylor, K., Lee, S.W., Ellis, B., Weiss, J., Kamper, D., 2014. Mechanical properties vary for different regions of the finger extensor apparatus. J. Biomech. 47, 3094–3099. https://doi.org/10.1016/j.jbiomech.2014.06.035.
Qiu, D., 2014. Original archival copy the impact of the joint posture on finger neuromechanics by. Illinois Institute of Technology.
Schmitz, A., Piovesan, D., 2016. Development of an open-source, discrete element knee model. IEEE Trans. Biomed. Eng. 63, 2056–2067. https://doi.org/10.1109/TBME.2016.2585926.
Suwannakhan, A., Tawonsawatruk, T., Meemon, K., 2016. Extensor tendons and variations of the medial four digits of hand: a cadaveric study. Surg. Radiol. Anat. 38, 1083–1093. https://doi.org/10.1007/S00276-016-1673-2/TABLES/5.
Triandafilou, K.M., Fischer, H.C., Towles, J.D., Kamper, D.G., Rymer, W.Z., 2011. Diminished capacity to modulate motor activation patterns according to task contributes to thumb deficits following stroke. J. Neurophysiol. 106, 1644–1651. https://doi.org/10.1152/jn.00936.2010.
Valero-Cuevas, F.J., Zajac, F.E., Burgar, C.G., 1998. Large index-fingertip forces are produced by subject-independent patterns of muscle excitation. J. Biomech. 31, 693–703. https://doi.org/10.1016/S0021-9290(98)00082-7.
Valero-Cuevas, F.J., Yi, J.W., Brown, D., McNamara, R.V., Paul, C., Lipson, H., 2007. The tendon network of the fingers performs anatomical computation at a macroscopic scale. IEEE Trans. Biomed. Eng. 54, 1161–1166. https://doi.org/10.1109/TBME.2006.889200.
Yeh, C.L., Sheu, Y.L., Kuo, P.L., Li, P.C., 2012. Investigation on anisotropy of elastic properties in tendon using shear wave elasticity imaging. IEEE Int. Ultrason. Symp. IUS 1359–1362. https://doi.org/10.1109/ULTSYM.2012.0339.
Zajac, F.E., 1989. Muscle and tendon: properties, models, scaling, and application to biomechanics and motor control. Crit. Rev. Biomed. Eng. 17, 359–411.